

1 **Recent decrease trend of atmospheric mercury concentrations in East China: the**
2 **influence of anthropogenic emissions**

3 Yi Tang^{1, 2}, Shuxiao Wang^{1, 2*}, Qingru Wu^{1, 2*}, Kaiyun Liu^{1, 2}, Long Wang³, Shu Li¹, Wei Gao⁴, Lei
4 Zhang⁵, Haotian Zheng^{1, 2}, Zhijian Li¹, Jiming Hao^{1, 2}

5

6 ¹ State Key Joint Laboratory of Environmental Simulation and Pollution Control, School of
7 Environment, Tsinghua University, Beijing 100084, China

8 ² State Environmental Protection Key Laboratory of Sources and Control of Air Pollution Complex,
9 Beijing 100084, China

10 ³ School of Environment and Energy, South China University of Technology, Guangzhou, 510006,
11 China

12 ⁴ Yangtze River Delta Center for Environmental Meteorology Prediction and Warning, Shanghai,
13 20030, China

14 ⁵ State Key Laboratory of Pollution Control & Resource Reuse, School of the Environment, Nanjing
15 University, Nanjing, 210023, China

16

17

18 * *Correspondence to:* Shuxiao Wang (shxwang@tsinghua.edu.cn)

19 Qingru Wu (qrwu@tsinghua.edu.cn)

20

21 **Abstract**

22 Measurements of gaseous elemental mercury (GEM), other air pollutants including SO₂, NO_x,
23 O₃, PM_{2.5}, CO, and meteorological conditions were carried out at Chongming Island in East China
24 from March 1 in 2014 to December 31 in 2016. During the sampling period, GEM concentrations
25 significantly decreased from 2.68±1.07 ng m⁻³ in 2014 (March to December) to 1.60 ±0.56 ng m⁻³
26 in 2016 (March to December). Monthly mean GEM concentration showed a significant decrease
27 with a rate of -0.60 ±0.08ng m⁻³ yr⁻¹ (R²=0.64, p<0.01 significance level). Combining the analysis
28 of potential source contribution function (PSCF), principle component analysis (PCA), and
29 emission inventory, we found that Yangtze River Delta (YRD) region was the dominant source
30 region of GEM in Chongming Island and the main source industries included coal-fired power
31 plants, coal-fired industrial boilers, and cement clinker production. We further quantified the effect
32 of emission change on the air Hg concentration variations at Chongming Island through a coupled
33 method of trajectory clusters and air Hg concentrations. It was found that the reduction of domestic
34 emissions was the main driver of GEM decline in Chongming Island, accounting for 70% of the
35 total decline. The results indicated that air pollution control policies targeting SO₂, NO_x and
36 particulate matter reductions had significant co-benefits on GEM.

37 **1 Introduction**

38 Mercury (Hg) is of crucial concern to public health and the global environment for its
39 neurotoxicity, long-distance transport, and bioaccumulation. The atmosphere is an important
40 channel for global Hg transport. Once atmospheric Hg deposits to the aquatic system, it can be
41 transformed into methylmercury (MeHg) which bio-accumulates through the food web and affects
42 the central nervous system of human beings (Mason et al., 1995). Hg is therefore on the priority list
43 of several international agreements and conventions dealing with environmental protection,
44 including the *Minamata Convention on Mercury*.

45 Atmospheric Hg exists in three operationally defined forms: gaseous elemental mercury (GEM),
46 gaseous oxidized mercury (GOM), and particulate-bound mercury (PBM). And the sum of GEM
47 and GOM is known as total gaseous mercury (TGM). In the atmosphere, Hg mainly presents as
48 GEM, accounting for over 95% of the total in the most observation sites (Fu et al., 2015; Li et al.,
49 2016; Zhang et al., 2017). GEM is stable and low solubility in the troposphere with a long residence
50 time and can be transported at regional and global scale (Lindberg et al., 2007). GEM can be
51 oxidized through photochemical reaction to GOM, which can be converted to PBM upon
52 adsorption/absorption on aerosol surfaces. GOM is more soluble than GEM, and PBM can be
53 quickly scavenged by both dry and wet deposition. Therefore, the residence time of both GOM and
54 PBM is shorter than that of GEM, generally several days to a few weeks for GOM and PBM and
55 0.5 – 2 year for GEM (Schroeder and Munthe, 1998).

56 The atmospheric Hg observation results are important evidences to assess the effect of Hg
57 emission control. During the past decades, significant decreases of GEM concentrations in Europe
58 and North America have been observed (Cole et al., 2013; Weigelt et al., 2015). Air Hg
59 concentrations in the northern hemisphere are reported to decline by 30-40% between 1990 and
60 2010 (Zhang Y et al., 2016). Such a decrease is consistent with the decrease in anthropogenic Hg
61 emissions inventory in Europe and North America (Streets et al., 2011). So far, most of the long-
62 term observations on the ground sites have been carried out in the developed countries. For the
63 developing countries such as China, limited atmospheric Hg observations have been carried out (Fu
64 et al., 2008b; Zhang H et al., 2016; Hong et al., 2016) and there is no official national observing

65 network of atmospheric Hg in mainland China. Therefore, there are few continuous multi-year
66 observation records of China's air Hg concentrations published (Fu et al., 2015).

67 China contributes to the largest Hg emissions in the world and will continue to be one significant
68 Hg emitter for global Hg emissions in the coming future (UNEP, 2013, Wu et al., 2016, Chen et al.,
69 2018; Pacyna et al., 2016). Large Hg emissions in China have led to the average air Hg
70 concentrations of $2.86 \pm 0.95 \text{ ng m}^{-3}$ (in the range of $1.60\text{-}5.07 \text{ ng m}^{-3}$) at the remote sites in China
71 (Fu et al., 2015). Such Hg concentration level is approximately 1.3 ng m^{-3} higher than the
72 background concentration of GEM in Northern Hemisphere (Zhang et al., 2016; Sprovieri et al.,
73 2017; Fu et al., 2015). In addition, the large Hg emissions in China will also impact the air Hg
74 concentrations in East Asia and even North America through long-range transport (Sung et al.,
75 2018; Zhang et al., 2017). Meanwhile, China has a great potential for Hg emission reduction during
76 implementation of the *Minamata Convention on Mercury* (Chen et al., 2018). Therefore, long-term
77 atmospheric Hg observations in China are critical to understand the Hg cycling at both regional and
78 global scale. China's Hg emissions had increased from 147 t yr^{-1} in 1978 to around 538 t yr^{-1} in 2010
79 due to the dramatic economic development (Zhang L et al., 2015; Wu et al., 2016; Hui et al., 2017).
80 Atmospheric Hg monitoring that spanned from 2002 to 2010 in Guiyang, southwestern China
81 reflected the increase of Hg emissions in China (Fu et al., 2011). However, atmospheric Hg
82 emissions in China was estimated to have been decreased since 2012 (Wu et al., 2016). This
83 decreasing trend needs to be confirmed by atmospheric Hg observations.

84 In this study, we measured GEM, other air pollutants (eg., $\text{PM}_{2.5}$ and NO_x), and meteorological
85 parameters (eg., temperature and wind speed) at a remote marine site of Chongming Island in East
86 China during 2014-2016. We analyzed annual and seasonal variations of GEM and the potential
87 impact factors. Combining the analysis of potential source contribution function (PSCF), principle
88 component analysis (PCA), emission inventory, and the potential source regions and source
89 industries of atmospheric Hg pollution at the monitoring site were identified. In addition, a method
90 which coupled trajectories and air Hg concentration was developed to assess the effect of Hg
91 emission changes from different regions on air GEM concentration variation at the monitoring site.

92 **2 Materials and methods**

93 **2.1 Site descriptions**

94 The monitoring remote site (31°32'13"N, 121°58'04"E, about 10 m above sea level) locates at the
95 top of weather station in Dongtan Birds National Natural Reserve, Chongming Island, China (Figure
96 1). As China's third largest island, Chongming Island is located at the east of Yangtze River Delta
97 region with a typical subtropical monsoon climate. It is rainy, hot, with southern and southeastern
98 winds in summer and is dry, cold, and with northwestern wind in winter. The dominant surface types
99 are farmland and wetland. There are no large anthropogenic emission sources in the island and no
100 habitants within 5 km distance from the site. The downtown Shanghai area is 50 km to the southwest
101 of the site.

102 **2.2 Sampling methods and analysis**

103 During the monitoring period, we used Tekran 2537X/1130/1135 instruments to monitor
104 speciated Hg in the atmosphere, which was widely used for air Hg observation in the world. The
105 sampling inlet was 1.5 m above the instrument platform. Continuous 5-minute of GEM was
106 measured by Tekran 2537X Hg vapor analyzer with the detection limit of 0.1 ng m⁻³ at a sampling
107 flow rate of 1.0 L min⁻¹ during two campaigns: March 1, 2014 to December 31, 2015 and March 26
108 to December 31, 2016. From July 5, 2015 to April 30 2016, the Tekran 1130/1135 speciation unit
109 was damaged by the rainstorm, the Tekran 2537X were operated without speciation units but with
110 PTFE filter to protect the instrument from particles and sea salt. Therefore, the observed
111 concentrations during July 2015-April 2016 were TGM concentrations indeed. However, the GOM
112 concentrations at Chongming Island accounted for less than 1% of TGM (TGM=GOM+GEM).
113 Thus, the GEM concentrations were approximated to TGM concentrations from July 2015 to April
114 2016.

115 The 2537X analyzer was calibrated automatically every 25 h using the internal Hg permeation
116 source inside the instrument, and the internal permeation source was calibrated every 12 months
117 with manual injection of Hg by a syringe from an external Hg source (module 2505). Two zero and
118 two span calibrations were performed for each calibration of gold trap A and B, respectively. The
119 difference between gold trap A and gold trap B was limited to ±10 %. The impactor plates and quartz

120 filter were changed in every two weeks. The soda lime was changed once a month. The denuders
121 were recoated once every two weeks following the procedure developed by Landis et al. (2002).

122 In our research, random uncertainties of individual measurement had been averaged out and the
123 systematic uncertainties need to be considered. The overall practically achievable systematic
124 uncertainty would be 10% considering that the instrument was not in ideal performance (Slemr et
125 al., 2015; Steffen et al., 2012). For example, slow deactivation of the traps, contamination of the
126 switching valves and leaks would increase the uncertainties but were difficult to quantify (Slemr et
127 al., 2015; Steffen et al., 2012). Because of the consistency of instrument and the quality
128 assurance/quality control have been paid special attention to during the sampling campaign, the
129 systematic differences of instrument did not affect the huge variation between 2014 and 2016.

130 During the sampling campaigns, PM_{2.5}, O₃, NO_x, CO and SO₂ were also monitored by Thermo
131 Scientific TEOM 1405D, Model 49i O₃ Analyzer, Model 48i CO Analyzer, Model 42i-TL NO_x
132 Analyzer and Model 43i SO₂ Analyzer, respectively. The detection limits of O₃, SO₂, NO_x, CO and
133 PM_{2.5} are 1.0, 0.5, 0.4, 0.04 and 0.1 µg m⁻³, respectively. The meteorological parameters including
134 air temperature, wind speed, and wind direction were measured by Vantage Pro2 weather station
135 (Davis Instruments). The instruments were tested and calibrated periodically. All data were hourly
136 averaged in this study.

137 **2.3 Sources apportionment of atmospheric Hg pollution**

138 2.3.1 PSCF model

139 To identify the source areas for pollutants with a relatively long lifetime such as GEM (Xu and
140 Akhtar, 2010), the PSCF values for mean GEM concentrations in grid cells in a study domain were
141 calculated by counting the trajectory segment endpoints that terminate within each cell. The number
142 of endpoints that fall in the *ij*-th cell are designated *n_{ij}*. The number of endpoints that GEM
143 concentrations corresponding to arrival time are higher than a specific criterion at the monitoring
144 site for the same cell is defined to be *m_{ij}*. The criterion in this study is set as the average Hg
145 concentration during our study period. The PSCF value for the *ij*-th cell is then defined as:

$$146 \quad PSCF_{ij} = \frac{m_{ij}}{n_{ij}} W_{ij} \quad (1)$$

147 where *W_{ij}* is an empirical weight to reduce the effects of grid cells with small *n_{ij}* values. In this study,

148 W_{ij} is defined as in the following formula, in which Avg is the mean n_{ij} of all grid cells with n_{ij}
149 greater than zero:

$$150 \quad W_{ij} = \begin{cases} 1.0 & n_{ij} > 2 * Avg \\ 0.7 & Avg < n_{ij} \leq 2 * Avg \\ 0.42 & 0.5 * Avg < n_{ij} \leq Avg \\ 0.17 & n_{ij} \leq 0.5 * Avg \end{cases} \quad (2)$$

151 The PSCF value indicates the probability of a grid cell through which polluted events occurs.
152 More method details can be found in the study of Polissar et al. (Polissar et al., 1999). In this study,
153 the domain that covered the potential contribution source region (105 °–135 °E, 15 °–45 °N) was
154 divided into 22500 grid cells with 0.2 °×0.2 ° resolution. 72-hour back trajectories were generated
155 hourly from 1 March, 2014 to 31 December, 2015 and from March 26 to December 31 in 2016 by
156 TrajStat, a software including HYSPLIT for trajectory calculation with trajectory statistics modules
157 (Wang et al., 2009). PSCF map was plotted using ArcGIS version 10.1.

158 2.3.2 Principal component analysis (PCA)

159 Principal component analysis between Hg and other pollutant concentrations was used to identify
160 potential sources. Strong positive loading (loading>0.40) with SO₂ and PM_{2.5} typically indicates the
161 impact of coal combustion, and strong positive loading with GEM and CO has often been used as
162 an indicator for regional transport because both pollutants have similar source and stable chemical
163 properties (Lin et al., 2006; Pirrone et al., 1996). In this study, PCA was applied to infer the possible
164 influencing factors of GEM in 2014 and 2016. Prior to analysis, each variable was normalized by
165 dividing its mean, and pollutant concentrations (SO₂, CO, NO_x, PM_{2.5}) were averaged to 1-h
166 sampling intervals to match the hourly Hg monitoring during sampling period. The results in 2016
167 had no CO data due to instrument broken. Statistics analyses were carried out by using SPSS 19.0
168 software.

169 **2.4 Quantification method of source contribution**

170 To further quantitatively assess the effect of change in emissions from different regions on air
171 concentrations variation at a certain monitoring site, a quantitative estimation method which coupled
172 trajectories with air Hg concentrations was developed. We firstly identified the trajectories by using
173 the National Oceanic and Atmospheric Administration (NOAA) Hybrid Single-Particle Lagrangian
174 Integrated Trajectory (HYSPLIT) model. The gridded meteorological data at a horizontal resolution
175 of 1 °×1 ° were obtained from the Global Data Assimilation System (GDAS) (Draxler and Hess,

176 1998). The starting height was set to be 500 m above ground level to represent the center height of
 177 boundary layer where pollutants are usually well mixed in boundary layer. Secondly, each trajectory
 178 was assigned with GEM concentration by matching the arriving time in Chongming site. Third, the
 179 backward trajectories which coupled with Hg concentrations were clustered into groups according
 180 to transport patterns by using NOAA HYSPLIT 4.7. Thus, the grouped clusters were applied to
 181 identify the Hg source regions. The Hg average concentration of the cluster j was calculated as
 182 equation (3). And, the trajectory weighted concentration in the cluster j as equation (4). At last, the
 183 contribution of reduction at a certain region on Hg concentration at monitoring sites in a certain
 184 period can be calculated as equation (5).

185

$$186 \quad C_{j,t} = \frac{\sum_{i=1}^n C_{i,j,t}}{\sum_{i=1}^n N_{i,j,t}} \quad (3)$$

$$187 \quad TWC_{j,t} = AR \times C_{j,t} \quad (4)$$

188 where N refers to a certain trajectory. j refers to a certain cluster. t is the studied period, and n is the
 189 number of trajectory. m is the number of cluster. C is the GEM concentration, ng m^{-3} . TWC refers
 190 to the trajectory weighted concentration, ng m^{-3} . In order to reduce the influence of trajectory
 191 changes in different region between calculated years, the average ratio (AR) was used here for
 192 calculating TWC.

$$193 \quad CR_j = \frac{TWC_{j,t_2} - TWC_{j,t_1}}{\sum_{j=1}^m TWC_{j,t_2} - \sum_{j=1}^m TWC_{j,t_1}} \quad (5)$$

194 where CR refers to the contribution of GEM reduction. t_1 and t_2 refers to the two period participating
 195 to comparison, namely year 2014 and 2016 in this study, respectively.

196 This approach is a simple method to quantify the influence of anthropogenic emissions on GEM
 197 concentration variation. It should be noted that uncertainties always exist in calculating trajectories,
 198 causing uncertainties in all trajectory-based approaches. Trajectory errors vary considerably in
 199 different situation. Draxler (1996) suggested uncertainties might be 10% of the travel distance.
 200 Besides, meteorological conditions were pretty similar in 2014 and 2016 so as to reduce the

201 interference from meteorology (Table S2).

202 **2.5 Regional atmospheric Hg emissions**

203 Regional anthropogenic GEM emissions by month were calculated by using both the technology-
204 based emission factor method and transformed normal distribution function method. Detailed
205 introduction of these two methods and the speciation profile of the emitted Hg for each sector were
206 described in our previous study (Wu et al., 2016). Conventional air pollutant (SO₂, PM_{2.5}, and NO_x)
207 emissions were calculated following the study of Zhao et al. (2013). The source regions included in
208 the emission inventory consisted of Shanghai, Jiangsu, Zhejiang, and Anhui provinces according to
209 the PSCF results (See section 3.3). The studied emission sectors included coal-fired power plants,
210 coal-fired industrial boilers, residential coal-combustion, cement clinker production, iron and steel
211 production, mobile oil combustion and other small emission sectors (eg., zinc smelting, lead
212 smelting, municipal solid incineration, copper smelting, aluminum production, gold production,
213 other coal combustion, stationary oil combustion, and cremation). The monthly Hg emissions were
214 mainly distributed according to fuel combustions or products productions by month (Table S1). For
215 small emission sectors, the annual emissions were equally distributed into monthly emissions.

216 The GEM emissions from natural sources E_N were calculated as following.

$$217 \quad E_N = \sum_i F_i \times A_i \times t \quad (6)$$

218 where F_i is a bi-directional Hg flux of canopy i , ng km⁻² yr⁻¹; A is the studied area, km²; t is the
219 studied year, yr. The bi-directional Hg flux was obtained from the study of Wang et al. (2016)
220 directly. It should be pointed out that the natural emission was a concept of net emission in this
221 manuscript, which reflected a net effect of two competing processes (Zhang, 2009): total Hg natural
222 emissions and total Hg deposition. The total natural emissions included primary natural release and
223 re-emission of legacy Hg stored in the terrestrial and water surface (Wang et al., 2016). When the
224 value is positive, it means the net effect is Hg emissions to air. Otherwise, Hg deposited.

225 **3 Results and discussions**

226 **3.1 Decreasing trends of atmospheric Hg during 2014-2016**

227 The average concentrations of GEM in 2014 (March to December), 2015 and 2016 (March to
228 December) were 2.68 ± 1.07 ng m⁻³, 2.14 ± 0.82 ng m⁻³, and 1.60 ± 0.56 ng m⁻³, respectively. The

229 GEM concentrations in 2014 were higher (t test, $p < 0.01$) than the Northern Hemisphere background
230 concentrations (about 1.5 ng m^{-3}) (Sprovieri et al., 2010) and those measured in other remote and
231 rural locations in China (Zhang H et al., 2015; Fu et al., 2008a; Fu et al., 2009). However, in 2016,
232 the GEM concentrations were similar to the background concentrations in the Northern Hemisphere.
233 During this period, monthly GEM concentrations showed a significant decrease with a rate of -0.60
234 $\pm 0.08 \text{ ng m}^{-3} \text{ yr}^{-1}$ ($R^2 = 0.64$, $p < 0.01$ significance level, $n = 32$) (Figure 2a). The amount of valid data
235 for each month was shown in Table S3. From another aspect, the trend decomposition of the GEM
236 concentration signal (signal = trend + seasonal + random) from March 2014 to December 2016 were
237 performed in Figure 2 (<https://anomaly.io/seasonal-trend-decomposition-in-r/>). By using this
238 method, we also observed a pronounced trend (Figure 2b) and the random was limited in the range
239 of $-0.24 - 0.24 \text{ ng m}^{-3}$ (Figure 2d).

240 One potential worry was that the calculated trend was sensitive to seasonal variation and the
241 missing data in January and February of 2016 might impact the downward trend. To evaluate the
242 impact of the missing data, we estimated the Hg concentrations in the missing months based on the
243 data of the same months in 2015 and 2017 (Figure S1). Combining the estimated data, we re-fitted
244 the Hg concentrations and downward trend still maintained robust and similar to the downward
245 trend in manuscript (Figure S1). Thus, we assumed that the missing data was not very important
246 and would not impact our main conclusion.

247 Table S4 showed the Hg variation trends in different regions. Significant decrease of GEM
248 concentrations in North hemisphere over the past two decades have been well documented (Weigelt
249 et al., 2015; Cole et al., 2013; Kim et al., 2016). All the stations in Table S4 used Tekran instruments
250 except for the observation in South Korea. Different instruments could cause potential differences
251 in the observation, but they were comparable and did not affect the conclusion of comparison in
252 downward trend (Slemr et al., 2015; Sprovieri et al., 2016). Weigelt et al. (2015) showed that GEM
253 concentrations decreased from 1.75 ng m^{-3} in 1996 to 1.4 ng m^{-3} in 2009 at Mace Head, Europe.
254 Ten-year trends of GEM concentrations at six ground-based sites in the Arctic and Canada also
255 showed a decreasing trend at a rate of $13\text{-}35 \text{ pg m}^{-3} \text{ y}^{-1}$ (Cole et al., 2013). In South Korea, the
256 observed GEM concentration also had significant decrease in recent years (Kim et al., 2016). In
257 South Africa, annual average GEM concentration at Cape Point decreased from 1.29 ng m^{-3} in

258 1996 to 1.19 ng m⁻³ in 2004 (Slemr et al., 2008) and were increasing from 0.93 ng m⁻³ in 2007
259 (Slemr et al., 2015) until 2016 (Martin et al., 2017). However, limited GEM monitoring sites and
260 relative short-time spans in China restricted the views of long-term trends in atmospheric Hg
261 concentration in this region. A preliminary assessment indicated that atmospheric Hg concentrations
262 in China kept increasing before 2012 (Fu et al., 2015). The decreasing trend observed in our study
263 was accordant with reported data in Mt. Changbai during 2014-2015 cited in the review of Fu et al.
264 (2015). The atmospheric Hg at Chongming was influenced by and in turn reflected regional Hg
265 emission and cycle. Although the decline in atmospheric Hg was observed in many sites of the
266 Northern Hemisphere, much sharper decrease of Hg concentrations was observed at Chongming in
267 our study. The specific reasons for the Hg concentration decrease in our study will be discussed in
268 section 3.4.

269 **3.2 Seasonal variation of GEM concentrations**

270 According to the decomposition result (Figure 2c), we observed strong seasonal cycle at
271 Chongming. The GEM concentrations were highest in July and lowest in September, so GEM
272 concentrations in the same month from different years were averaged to understand the detrended
273 seasonal circle (Figure 3). The error bars in the Figure 3 meant the standard deviation of the monthly
274 average. Observed GEM concentrations showed an obvious seasonal cycle. The mean GEM
275 concentration in warm season (from April to September) was 0.29 ng m⁻³ higher than that in cold
276 season. Such seasonal variation trend was also observed at Nanjing, Miyun, Mt. Ailao, Mt. Waliguan,
277 and Shangri-La (Zhang et al., 2013; Zhang et al., 2016; Fu et al., 2015; Zhu et al., 2012). On the
278 other hand, the GEM concentrations at Mt. Gongga, Mt. Daimei, Mt. Leigong, and Mt. Changbai in
279 China were relatively higher in cold seasons. The average of atmospheric Hg concentrations in the
280 north hemisphere also had a trough value in summer (Sprovieri et al., 2016).

281 Seasonal variations of GEM concentration were generally attributed to the following factors,
282 including natural and anthropogenic emissions, atmospheric chemical reaction, and air mass
283 transport. The higher Hg concentrations in cold seasons in Mt. Leigong were mainly explained by
284 coal-combustion for urban and residential heating during cold seasons. Whereas, increasing solar
285 radiation and soil/air temperature dominated the higher Hg concentrations in Mt. Ailao. In addition,
286 sites in southern, eastern, and northeastern China were also impacted from anthropogenic

287 emissions of GEM from the north and west by the northerly winter monsoon while the sites located
288 in western, southwestern, and northern China were impacted in the warm season (Fu et al., 2015).
289 As to most sites in the northern hemisphere, high wet Hg precipitation induced probably by faster
290 GEM oxidation led to lower Hg concentrations in summer.

291 Source emission was one significant factor on GEM concentrations in the air. The GEM
292 concentrations at a remote site were generally regarded under the impact of regional emissions.
293 Therefore, the emissions in the YRD regions (Anhui, Zhejiang, Jiangsu, and Shanghai) were
294 calculated during 2014-2016. However, the anthropogenic emissions were in the range of 2.5-2.7 t,
295 which was almost unchanged. Compared to the anthropogenic emissions, we observed almost
296 synchronized trends between natural emissions and air Hg concentrations in Figure 4. The natural
297 emissions showed a huge seasonal variation, from -5.4 t to 8.4 t. The largest natural emissions were
298 observed in summer when the highest GEM concentrations were monitored. In the autumn, the
299 natural emissions performed as the largest deposition direction amount and the GEM concentrations
300 were the lowest in the whole year. Therefore, natural emissions instead of anthropogenic emissions
301 were supposed to be one significant factor of the seasonal cycle of GEM concentrations (Figure 4).
302 The seasonal trend of natural emissions was closely related with the canopy types in YRD areas,
303 where widely subtropical forests, paddy field, and dry farming were observed (Figure S2). The high
304 temperature will speed up decomposition of organic compound in soil, which leads to Hg emissions
305 from farmland and forest in YRD region in summer (Luo et al., 2016; Yu et al., 2017). In autumn
306 and winter, with the decrease of temperature (Table S2), the role of soil changed from Hg source to
307 sink, which reduced the Hg concentrations in the air (Wang et al., 2016). At the same time, the
308 growing vegetation in autumn also absorbed air Hg, resulting lower Hg concentrations compared to
309 that in winter. Transport also overall enhanced the observed seasonal variation of GEM
310 concentrations at Chongming Island. According to the statistics of backward trajectories in section
311 3.4, the GEM concentrations in the air mass which did not pass via the YRD regions also showed
312 high GEM concentration in warm season in 2014 (Figure S3).

313 From Figure 2, we also observed more pronounced seasonal variation in 2014, which could be
314 attributed to the lower wet deposition and GEM oxidation. On one aspect, as a costal site, the
315 Chongming Island was abundant with $\bullet\text{OH}$. The increase of O_3 concentration from the summer of

316 2014 to 2016 may contribute to a higher oxidation of GEM in 2016. On another aspect, higher wet
317 Hg deposition in summer was approximately 6.6 times of that in the winter at Chongming (Zhang
318 et al., 2010). Meanwhile, the rainfall in 2016 summer (546 mm) was higher than the rainfall in
319 2014 (426 mm). Therefore, the higher oxidation and wet deposition rate of Hg in the summer of
320 2016 would reduce the concentration difference between summer and winter, which led to a less
321 pronounced seasonal variation in 2016. Meanwhile, the higher oxidation and wet deposition in
322 2016 also contributed to the downward trend of GEM by reducing the seasonality in spring and
323 summer (Figure S3).

324 **3.3 Source apportionment of atmospheric Hg pollutions**

325 According to the PSCF result, YRD region, including Shanghai, Jiangsu, Anhui, and Zhejiang
326 provinces, was the dominant source region in both 2014 and 2016 (Figure 5). Therefore, Hg
327 emissions from these areas would contribute to high proportion of Hg pollution at Chongming Island.
328 The offshore area mainly around Jiangsu province also had a high PSCF value because some
329 trajectories from North China, especially Shandong province, transport to Chongming Island
330 through this area. Compared to the result in 2014, the PSCF value had an obvious decline in East
331 China Sea in 2016. The decline from the East China Sea may be contributed by the downward trend
332 of GEM concentrations in South Korea and Japan (Kim et al., 2016; Kim et al., 2013), where the
333 anthropogenic Hg emissions of Japan and South Korea were reduced by 13% and 4% during 2010-
334 2015, respectively (UNEP 2013; UNEP 2018). The air mass from Japan and South Korea would
335 pass through the East China Sea to Chongming.

336 PCA method was applied to preliminarily identify the potential source sectors. In the studied
337 period, totally 2 factors were identified in 2014 and 2016, respectively. The factor 1 had strong
338 factor loadings of GEM, SO₂, NO_x, CO, and PM_{2.5} in both 2014 and 2016 (No CO data in 2016 due
339 to equipment problems). The factor 1 accounted for 49% variance in 2014 and 50% variance in
340 2016 (Table 1). The results indicated common significant source sectors of the above five air
341 pollutants, which could also be proven from emission inventories (Table 2). The dominant source
342 industries included coal-fired power plants, coal-fired industrial boilers, and cement clinker
343 production. The PCA results showed that anthropogenic emissions were the main sources of GEM
344 during the sampling period.

345 The factor 2 in both 2014 and 2016 had a strong positive loading on O₃ and negative loading on
346 NO_x. Considering the low loading of CO and high loading of O₃, the factor 2 represented the
347 transport of air mass from the stratosphere (Fishman and Seiler, 1983; Jaffe, 2010). The air mass
348 from stratosphere would increase the O₃ concentration. O₃ reacted with NO, which made a negative
349 correlation with NO. However, the low loading on GEM of factor 2 indicated that Factor 2 had no
350 relationship with GEM concentrations at Chongming from the aspect of whole year data.

351 **3.4 The influence of anthropogenic emissions**

352 To further understand the reason of the downward trend, we firstly compared the meteorological
353 conditions in both 2014 and 2016. We noted that the difference of annual temperature, solar radiation,
354 and relative humidity were constrained in the range of 17.13 ± 7.48 °C, 165.55 ± 45.87 W m⁻² and
355 $75.38 \pm 5.82\%$, respectively (Table S2). The coefficients of variation for annual mean of these
356 meteorological conditions in 2014 and 2016 were 2.6%, 6.7% and 0.2%, respectively. In addition,
357 the wind rose was similar, and the dominating wind was from SE in both 2014 and 2016 (Figure
358 S4). The HYSPLIT results also provided similar trajectories in 2014 and 2016 (Figure 6). Therefore,
359 we assumed that the meteorological condition was not the dominant reason of GEM decline at
360 Chongming site.

361 To further quantify the driver of GEM decline, a trajectory-based analysis method was used in
362 this study. The 72-h air mass back trajectories were calculated using HYSPLIT for every 8 hours
363 starting at the observation site. Approximately 918 and 832 trajectories were calculated in sampling
364 period in 2014 (Mar 1 to Dec 31, 2014) and 2016 (Mar 26 to Dec 31, 2016), respectively. The
365 trajectories were grouped into 3 clusters in each year according to geographical regions (Figure 6).
366 The first cluster of trajectories mainly passed through the regions (eg., North China) north and
367 northwest to Chongming Island before arriving to our monitoring site, which was denoted as cluster
368 NCP. The second cluster mainly passed YRD region to Chongming, which was signed as cluster
369 SW-YRD. The third type mainly originated from the East China Seas, South Korea, Japan and
370 Northeast Asia continent, and then arrived to our monitoring sites directly without passing the
371 mainland China. This type of trajectories was named as cluster ABROAD. Some trajectories
372 originated from the East China Sea and crossed the mainland China before arriving Chongming
373 were grouped into cluster NCP or SW-YRD depending on the regions it crossed. The trajectories

374 for each of the three clusters in 2014 and 2016 were shown in Table 3.

375 Table 3 showed the detail statistics data of the three classifications. From 2014 to 2016, the whole
376 China region (NCP, SW-YRD) contributed to 70% of GEM decline at Chongming Island.
377 Considering downward trend of emission inventory and atmospheric pollutant from 2014 to 2016
378 in NCP and SW-YRD region (Table S5, Table S6), the reason of downward trend could be attributed
379 to the effectiveness of existing air pollution control measures in China (SC, 2013; MEP, 2014).
380 Meanwhile, the cluster NCP, cluster SW-YRD, and cluster ABROAD caused 26%, 44%, and 30%
381 for GEM decline, respectively (Table 3). The cluster SW-YRD contributed to 44% of reduction,
382 suggesting that air pollution controls on anthropogenic emissions in YRD region dominated the
383 recent decrease of GEM concentrations at Chongming site. The largest decline of Hg concentration
384 (1.32 ng m^{-3}) was also observed in the cluster SW-YRD, which demonstrated the efficiency of
385 emission reduction in YRD region (Table S5, Table S6). Moreover, ABROAD region caused 30%
386 of GEM decline from 2014 to 2016, which implied global effort on atmospheric Hg emission control
387 under the guidance of *Minamata Convention on Mercury*.

388 **4 Conclusion**

389 Atmospheric Hg was continuously measured for three years at a regional background site in the
390 YRD region. During the sampling period, a downward trend for GEM concentrations (-0.60 ± 0.08
391 $\text{ng m}^{-3} \text{ y}^{-1}$) at Chongming Island was observed. The seasonal GEM cycle was dominated by the
392 natural emissions while the annual GEM concentration trend was mainly impacted by anthropogenic
393 emissions. By using a new approach that considers both cluster frequency and the Hg concentration
394 associated with each cluster, we quantified that atmospheric Hg from NCP region, SW-YRD region,
395 and ABROAD region caused 26%, 44%, and 30% decline of GEM concentrations at Chongming
396 monitoring site during 2014-2016, respectively. The result suggested that reduction of
397 anthropogenic emissions in mainland China was the main cause of the recent decreasing trend of
398 GEM concentration at Chongming site. The air pollution control policies in China, especially the
399 pollution control in the coal-fired power plants, coal-fired industrial boilers, and cement clinker
400 production in YRD region and Shandong province, received significant co-benefit of atmospheric
401 Hg emission reductions. On the other hand, emission reduction from the ABROAD region, where

402 clusters arrived to Chongming monitoring site directly without passing the mainland China, implied
403 global effort on atmospheric Hg emission control under the guidance of *Minamata Convention on*
404 *Mercury*. Considering that the *Minamata Convention on Mercury* had come into force in 2017,
405 continuous long-term observation of atmospheric Hg in China will be required for the assessment
406 of policy effectiveness.

407

408 *Data availability.* All data are available from the authors upon request.

409

410 *Competing interests.* The authors declare that they have no conflict of interest.

411

412 *Acknowledge.* This work is sponsored by the Natural Science Foundation of China (No. 21607090),
413 Major State Basic Research Development Program of China (973 Program) (No. 2013CB430000),
414 National Key R&D Program of China (No. 2016YFC0201900)

415

416

417

418

419

420 **References**

- 421 Cole, A. S., Steffen, A., Pfaffhuber, K. A., Berg, T., Pilote, M., Poissant, L., Tordon, R., and Hung,
422 H.: Ten-year trends of atmospheric mercury in the high Arctic compared to Canadian sub-Arctic
423 and mid-latitude sites, *Atmospheric Chemistry and Physics*, 13, 1535-1545, 2013.
- 424 Chen, L., Zhang, W., Zhang, Y., Tong, Y., Liu, M., Wang, H., Xie, H., and Wang, X.: Historical and
425 future trends in global source-receptor relationships of mercury, *Science of the Total Environment*,
426 610-611, 24-31, 2018.
- 427 Draxler, R. R.: Trajectory Optimization for Balloon Flight Planning, *International Journal for*
428 *Numerical Methods in Fluids*, 5, 13-23, 1996.
- 429 Draxler, R. R., and Hess, G. D.: An overview of the hysplit-4 modeling system for trajectories,
430 *Australian Meteorological Magazine*, 47, 295-308, 1998.
- 431 Fishman J, Seiler W. Correlative Nature of Ozone and Carbon Monoxide in the Troposphere:
432 Implications for the Tropospheric Ozone Budget. *Journal of Geophysical Research*, 88(C6), 1983.
- 433 Fu, X. W., Feng, X. B., Zhu, W. Z., Wang, S. F., and Lu, J. L.: Total gaseous mercury concentrations
434 in ambient air in the eastern slope of Mt. Gongga, South-Eastern fringe of the Tibetan plateau, China,
435 *Atmospheric Environment*, 42, 970-979, 2008a.
- 436 Fu, X. W., Feng, X. B., Zhu, W. Z., Zheng, W., Wang, S. F., and Lu, J. Y.: Total particulate and
437 reactive gaseous mercury in ambient air on the eastern slope of the Mt. Gongga area, China, *Applied*
438 *Geochemistry*, 23, 408-418, 2008b.
- 439 Fu, X. W., Feng, X. B., Wang, S., Rothenberg, S., Shang, L., Li, Z., and Qiu, G.: Temporal and
440 spatial distributions of total gaseous mercury concentrations in ambient air in a mountainous area
441 in southwestern China: implications for industrial and domestic mercury emissions in remote areas
442 in China, *Science of the Total Environment*, 407, 2306-2314, 2009.
- 443 Fu, X. W., Feng, X. B., Qiu, G. L., Shang, L. H., and Zhang, H.: Speciated atmospheric mercury
444 and its potential source in Guiyang, China, *Atmospheric Environment*, 45, 4205-4212, 2011.
- 445 Fu, X. W., Zhang, H., Yu, B., Wang, X., Lin, C. J., and Feng, X. B.: Observations of atmospheric
446 mercury in China: a critical review, *Atmospheric Chemistry and Physics*, 15, 9455-9476, 2015.
- 447 Hong, Q. Q., Xie, Z. Q., Liu, C., Wang, F. Y., Xie, P. H., Kang, H., Xu, J., Wang, J. C., Wu, F. C.,

448 He, P. Z., Mou, F. S., Fan, S. D., Dong, Y. S., Zhan, H. C., Yu, X. W., Chi, X. Y., and Liu, J. G.:
449 Speciated atmospheric mercury on haze and non-haze days in an inland city in China, *Atmospheric*
450 *Chemistry and Physics*, 16, 13807-13821, 2016.

451 Hui, M. L., Wu, Q. R., Wang, S. X., Liang, S., Zhang, L., Wang, F. Y., Lenzen, M., Wang, Y. F., Xu,
452 L. X., Lin, Z. T., Yang, H., Lin, Y., Larssen, T., Xu, M., and Hao, J. M.: Mercury flows in China and
453 global drivers, *Environmental Science & Technology*, 51, 222-231, 2017.

454 Jaffe, D.: Relationship between surface and free tropospheric ozone in the western U.S.,
455 *Environmental Science & Technology*, 45, 432-438, 2010.

456 Kim, K.-H., Yoon, H.-O., Brown, R. J. C., Jeon, E.-C., Sohn, J.-R., Jung, K., Park, C.-G., and Kim,
457 I.-S.: Simultaneous monitoring of total gaseous mercury at four urban monitoring stations in Seoul,
458 Korea, *Atmospheric Research*, 132-133, 199-208, 2013.

459 Kim, K. H., Brown, R. J. C., Kwon, E., Kim, I. S., and Sohn, J. R.: Atmospheric mercury at an urban
460 station in Korea across three decades, *Atmospheric Environment*, 131, 124-132, 2016.

461 Landis, M. S., Stevens, R. K., Schaedlich, F., and Prestbo, E. M.: Development and characterization
462 of an annular denuder methodology for the measurement of divalent inorganic reactive gaseous
463 mercury in ambient air, *Environmental Science & Technology*, 36, 3000-3009, 2002.

464 Lindberg, S., Bullock, R., Ebinghaus, R., Engstrom, D., Feng, X. B., Fitzgerald, W., Pirrone, N.,
465 Prestbo, E., and Seigneur, C.: A synthesis of progress and uncertainties in attributing the sources of
466 mercury in deposition, *Ambio*, 36, 19, 2007.

467 Li, S., Gao, W., Wang, S. X., Zhang, L., Li, Z. J., Wang, L., and Hao, J. M.: Characteristics of
468 Speciated Atmospheric Mercury in Chongming Island, Shanghai, *Environmental Science* 37, 3290
469 - 3299, 2016.

470 Luo, Y., Duan, L., Driscoll, C. T., Xu, G., Shao, M., Taylor, M., Wang, S. X., and Hao, J. M.:
471 Foliage/atmosphere exchange of mercury in a subtropical coniferous forest in south China, *Journal*
472 *of Geophysical Research Biogeosciences*, 121, 2016.

473 Martin, L. G., Labuschagne, C., Brunke, E. G., Weigelt, A., Ebinghaus, R., and Slemr, F.: Trend of
474 atmospheric mercury concentrations at Cape Point for 1995–2004 and since 2007, *Atmospheric*
475 *Chemistry and Physics*, 17, 2393-2399, 2017.

476 Mason, R. P., Reinfelder, J. R., and Morel, F. M. M.: Bioaccumulation of mercury and

477 methylmercury, Springer Netherlands, 915-921 pp., 1995.

478 Ministry of Environmental Protection (MEP) and State Administration for Quality Supervision and
479 Inspection and Quarantine (AQSIQ): Emission standard of air pollutants for boilers, MEP, Beijing,
480 China, 2014.

481 Pirrone, N., Keeler, G. J., and Nriagu, J. O.: Regional differences in worldwide emissions of mercury
482 to the atmosphere, *Atmospheric Environment*, 30, 2981-2987, 1996.

483 Polissar, A. V., Hopke, P. K., Paatero, P., Kaufmann, Y. J., Hall, D. K., Bodhaine, B. A., Dutton, E.
484 G., and Harris, J. M.: The aerosol at Barrow, Alaska: long-term trends and source locations,
485 *Atmospheric Environment*, 33, 2441-2458, 1999.

486 State Council of the People's Republic of China (SC): Action plan of national air pollution
487 prevention and control, SC, Beijing, China, 2013.

488 Schroeder, W. H., and Munthe, J.: Atmospheric mercury—An overview, *Atmospheric Environment*,
489 32, 809-822, 1998.

490 Slemr, F., Angot, H., Dommergue, A., Magand, O., Barret, M., Weigelt, A., Ebinghaus, R., Brunke,
491 E. G., Pfaffhuber, K. A., Edwards, G., Howard, D., Powell, J., Keywood, M., and Wang, F.:
492 Comparison of mercury concentrations measured at several sites in the Southern Hemisphere,
493 *Atmospheric Chemistry and Physics*, 15, 3125-3133, 2015.

494 Sprovieri, F., Pirrone, N., Ebinghaus, R., Kock, H., and Dommergue, A.: A review of worldwide
495 atmospheric mercury measurements, *Atmospheric Chemistry and Physics*, 10, 8245-8265, 2010.

496 Streets, D. G., Devane, M. K., Lu, Z., Bond, T. C., Sunderland, E. M., and Jacob, D. J.: All-Time
497 releases of mercury to the atmosphere from human activities, *Environmental Science & Technology*,
498 45, 10485-10491, 2011.

499 Sprovieri, F., Pirrone, N., Bencardino, M., amp, apos, Amore, F., Carbone, F., Cinnirella, S.,
500 Mannarino, V., Landis, M., Ebinghaus, R., Weigelt, A., Brunke, E.-G., Labuschagne, C., Martin, L.,
501 Munthe, J., Wängberg, I., Artaxo, P., Morais, F., Barbosa, H. d. M. J., Brito, J., Cairns, W., Barbante,
502 C., Diéguez, M. d. C., Garcia, P. E., Dommergue, A., Angot, H., Magand, O., Skov, H., Horvat, M.,
503 Kotnik, J., Read, K. A., Neves, L. M., Gawlik, B. M., Sena, F., Mashyanov, N., Obolkin, V., Wip,
504 D., Feng, X. B., Zhang, H., Fu, X., Ramachandran, R., Cossa, D., Knoery, J., Maruszczak, N.,
505 Nerentorp, M., and Norstrom, C.: Atmospheric mercury concentrations observed at ground-based

506 monitoring sites globally distributed in the framework of the GMOS network, *Atmospheric*
507 *Chemistry and Physics*, 16, 11915-11935, 2016.

508 Sprovieri, F., Pirrone, N., Bencardino, M., amp, apos, Amore, F., Angot, H., Barbante, C., Brunke,
509 E.-G., Arcega-Cabrera, F., Cairns, W., Comero, S., Di éguez, M. d. C., Dommergue, A., Ebinghaus,
510 R., Feng, X. B., Fu, X., Garcia, P. E., Gawlik, B. M., Hageström, U., Hansson, K., Horvat, M.,
511 Kotnik, J., Labuschagne, C., Magand, O., Martin, L., Mashyanov, N., Mkololo, T., Munthe, J.,
512 Obolkin, V., Ramirez Islas, M., Sena, F., Somerset, V., Spandow, P., Vardè M., Walters, C.,
513 Wängberg, I., Weigelt, A., Yang, X., and Zhang, H.: Five-year records of mercury wet deposition
514 flux at GMOS sites in the Northern and Southern hemispheres, *Atmospheric Chemistry and Physics*,
515 17, 2689-2708, 2017

516 Steffen, A., Scherz, T., Olson, M., Gay, D., and Blanchard, P.: A comparison of data quality control
517 protocols for atmospheric mercury speciation measurements, *J Environ Monit*, 14, 752-765, 2012.

518 Sung, J.-H., Roy, D., Oh, J.-S., Back, S.-K., Jang, H.-N., Kim, S.-H., Seo, Y.-C., Kim, J.-H., Lee, C.
519 B., and Han, Y.-J.: Trans-boundary movement of mercury in the Northeast Asian region predicted
520 by CAMQ-Hg from anthropogenic emissions distribution, *Atmospheric Research*, 203, 197-206,
521 2018.

522 Arctic Monitoring and Assessment Programme and United Nations Environment Programme
523 (AMAP/UNEP): Global Hg assessment 2013: sources, emissions, releases and environmental
524 transport, AMAP/UNEP, Geneva, Switzerland, 2013

525 Arctic Monitoring and Assessment Programme and United Nations Environment Programme
526 (AMAP/UNEP): Global mercury assessment 2018 - draft technical background document,
527 AMAP/UNEP, Geneva, Switzerland, 2018.

528 Wang, X., Lin, C.-J., Yuan, W., Sommar, J., Zhu, W., and Feng, X.: Emission-dominated gas
529 exchange of elemental mercury vapor over natural surfaces in China, *Atmospheric Chemistry and*
530 *Physics*, 16, 11125-11143, 2016.

531 Wang, Y. Q., Zhang, X. Y., and Draxler, R. R.: TrajStat: GIS-based software that uses various
532 trajectory statistical analysis methods to identify potential sources from long-term air pollution
533 measurement data, Elsevier Science Publishers B. V., 938-939 pp., 2009.

534 Weigelt, A., Ebinghaus, R., Manning, A. J., Derwent, R. G., Simmonds, P. G., Spain, T. G., Jennings,

535 S. G., and Slemr, F.: Analysis and interpretation of 18 years of mercury observations since 1996 at
536 Mace Head, Ireland, *Atmospheric Environment*, 100, 85-93, 2015.

537 Wu, Q., Wang, S., Li, G., Liang, S., Lin, C. J., Wang, Y., Cai, S., Liu, K., and Hao, J.: Temporal
538 trend and spatial distribution of speciated atmospheric mercury emissions in China during 1978-
539 2014, *Environmental Science & Technology*, 50, 13428-13435, 2016.

540 Xu, X., and Akhtar, U. S.: Identification of potential regional sources of atmospheric total gaseous
541 mercury in Windsor, Ontario, Canada using hybrid receptor modeling, *Atmospheric Chemistry and
542 Physics*, 10, 7073-7083, 2010.

543 Yu Q, Luo Y, Wang S, Wang Z, Hao J, Duan L. Gaseous Elemental Mercury (GEM) Fluxes over
544 Canopy of Two Typical Subtropical Forests in South China. *Atmospheric Chemistry and Physics*,
545 18(1), 495-509, 2018.

546 Zhang, G. Y., Zhou, L. M., Zheng, X. M., and Huang, W. D.: Temporal distribution and potential
547 hazards of wet deposition mercury in Yangtze River Estuary, *Urban Environmental & Urban Ecology*,
548 1-4, 2010.

549 Zhang, H., Fu, X. W., Lin, C. J., Wang, X., and Feng, X. B.: Observation and analysis of speciated
550 atmospheric mercury in Shangri-La, Tibetan Plateau, China, *Atmospheric Chemistry and Physics*,
551 15, 653-665, 2015.

552 Zhang, H., Fu, X. W., Lin, C.-J., Shang, L. H., Zhang, Y. P., Feng, X. B., and Lin, C.: Monsoon-
553 facilitated characteristics and transport of atmospheric mercury at a high-altitude background site
554 in southwestern China, *Atmospheric Chemistry and Physics*, 16, 13131-13148, 2016.

555 Zhang, L., Wang, S. X., Wang, L., Wu, Y., Duan, L., Wu, Q. R., Wang, F. Y., Yang, M., Yang, H.,
556 Hao, J. M., and Liu, X.: Updated emission inventories for speciated atmospheric mercury from
557 anthropogenic sources in China, *Environmental Science & Technology*, 49, 3185-3194, 2015.

558 Zhang, L. M., Wright, L. P., and Blanchard, P.: A review of current knowledge concerning dry
559 deposition of atmospheric mercury, *Atmospheric Environment*, 43, 5853-5864, 2009.

560 Zhang, Y. X., Jacob, D. J., Horowitz, H. M., Chen, L., Amos, H. M., Krabbenhoft, D. P., Slemr, F.,
561 St Louis, V. L., and Sunderland, E. M.: Observed decrease in atmospheric mercury explained by
562 global decline in anthropogenic emissions, *Proceedings of the National Academy of Sciences of the
563 United States of America*, 113, 526, 2016.

564 Zhao, B., Wang, S. X., Liu, H., Xu, J. Y., Fu, K., Klimont, Z., Hao, J. M., He, K. B., Cofala, J., and
565 Amann, M.: NO_x emissions in China: historical trends and future perspectives, *Atmospheric*
566 *Chemistry and Physics*, 13, 9869-9897, 2013.

567 Zhu, J., Wang, T., Talbot, R., Mao, H., Hall, C. B., Yang, X., Fu, C., Zhuang, B., Li, S., Han, Y., and
568 Huang, X.: Characteristics of atmospheric total gaseous mercury (TGM) observed in urban Nanjing,
569 China, *Atmospheric Chemistry and Physics*, 12, 12103-12118, 2012.

570

571 **Figure citation**

572 **Figure 1.** The location of the Chongming monitoring site in Shanghai, China

573 **Figure 2.** Monthly average GEM concentrations during the studied period (a) observed monthly
574 GEM concentrations (b) GEM trend after decomposition (c) GEM seasonality after decomposition
575 (d) GEM random after decomposition

576 Note: The observed concentrations during July 2015-April 2016 were TGM concentrations indeed
577 due to the problems of Tekran 1130/1135. However, the GOM concentrations at Chongming Island
578 accounted for less than 1% of TGM. Thus, the GEM concentrations were approximated to TGM
579 concentrations during July 2015-April 2016.

580 **Figure 3.** Monthly variations of GEM concentration at remote sites in China

581 **Figure 4.** Seasonal cycle of GEM concentrations, anthropogenic and natural emissions during 2014-
582 2016. The error bars represent the standard deviation of seasonal average. Negative values of natural
583 emissions represent mercury deposition and positive values of natural emissions represent natural
584 emissions.

585 **Figure 5.** Source regions of GEM at monitoring site from PSCF model in 2014(a) and 2016(b)

586 **Figure 6.** The back trajectories map for cluster NCP, SW-YRD and ABROAD in 2014(a) and
587 2016(b)

588 (NCP – North China Plain; SW-YRD –Southwest region and Yangtze River Delta; ABROAD –
589 Abroad)

590 **Table citation**
591 **Table 1.** PCA component loading of GEM and the co-pollutants
592 **Table 2.** Main air pollutant emitted by the different sector in YRD region in 2014
593 **Table 3.** The statistics of cluster and estimated contribution of GEM reduction in 2014 and 2016
594
595

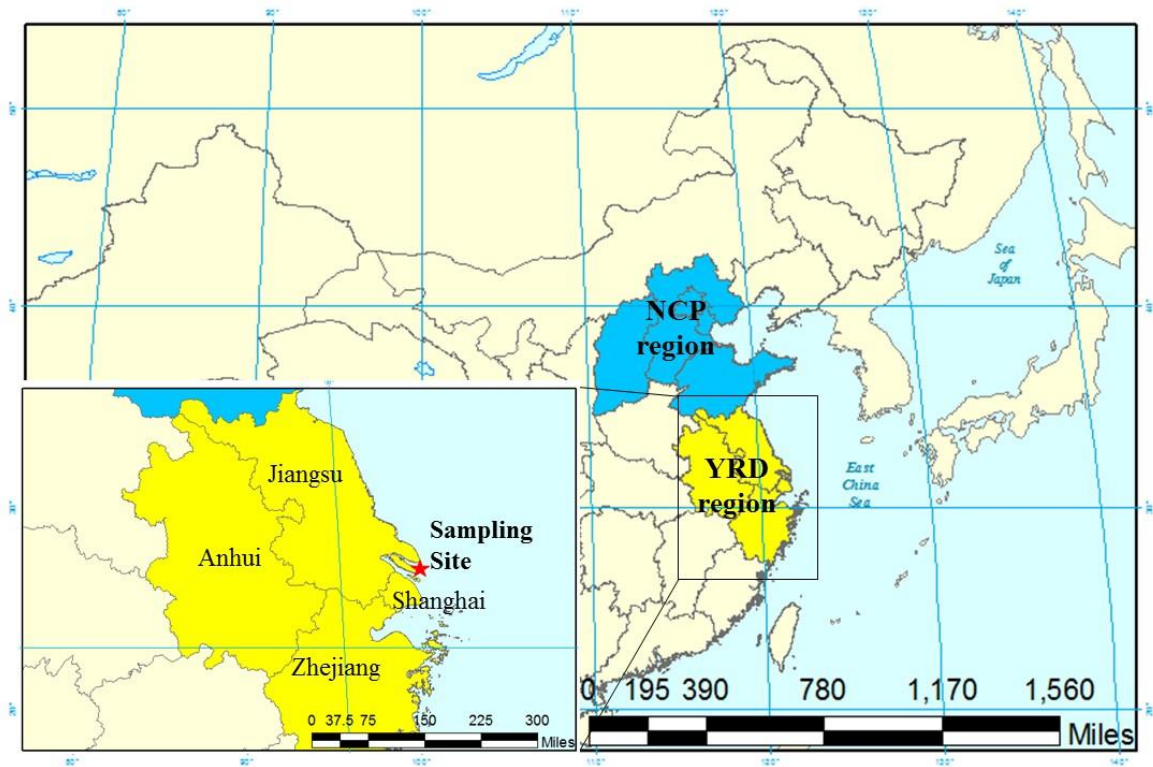
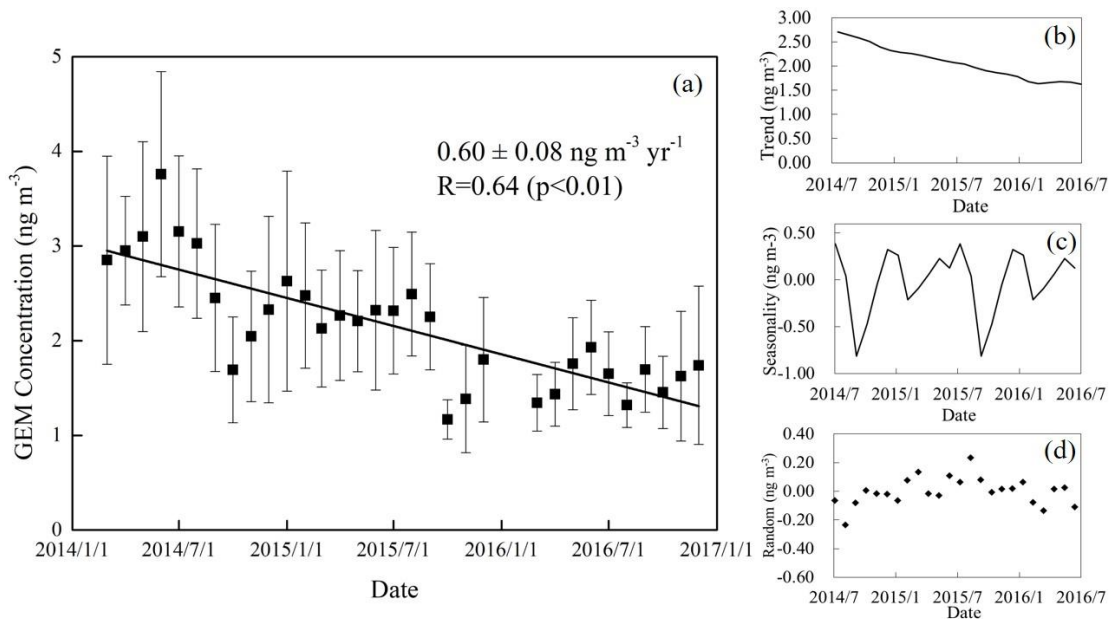


Figure 1. The location of the Chongming monitoring site in Shanghai, China

596

597



598
 599
 600
 601
 602
 603
 604
 605
 606

Figure 2. Monthly average GEM concentrations during the studied period (a) observed monthly GEM concentrations (b) GEM trend after decomposition (c) GEM seasonality after decomposition (d) GEM random after decomposition

Note: The observed concentrations during July 2015-April 2016 were TGM concentrations indeed due to the problems of Tekran 1130/1135. However, the GOM concentrations at Chongming Island accounted for less than 1% of TGM. Thus, the GEM concentrations were approximated to TGM concentrations during July 2015-April 2016.

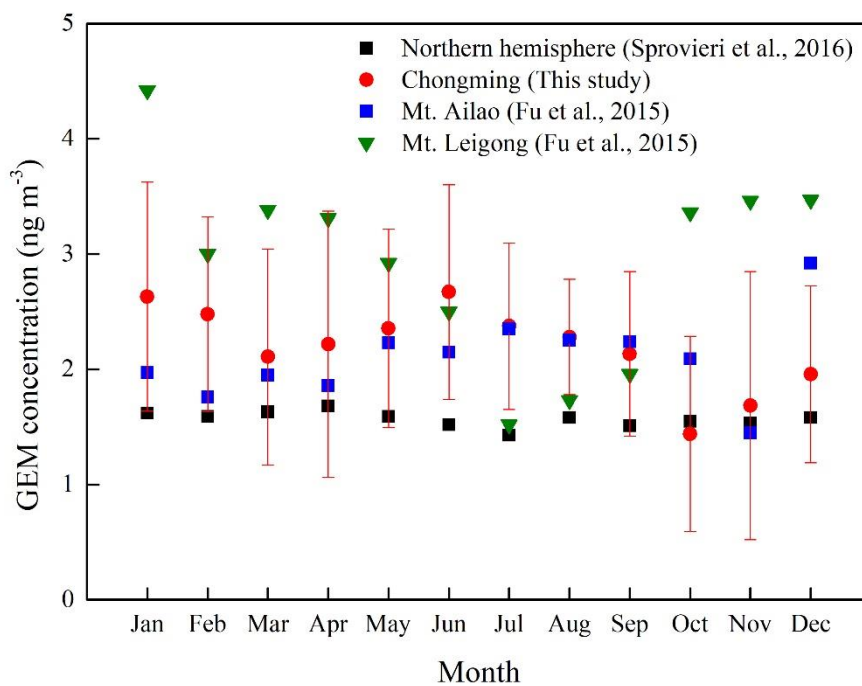
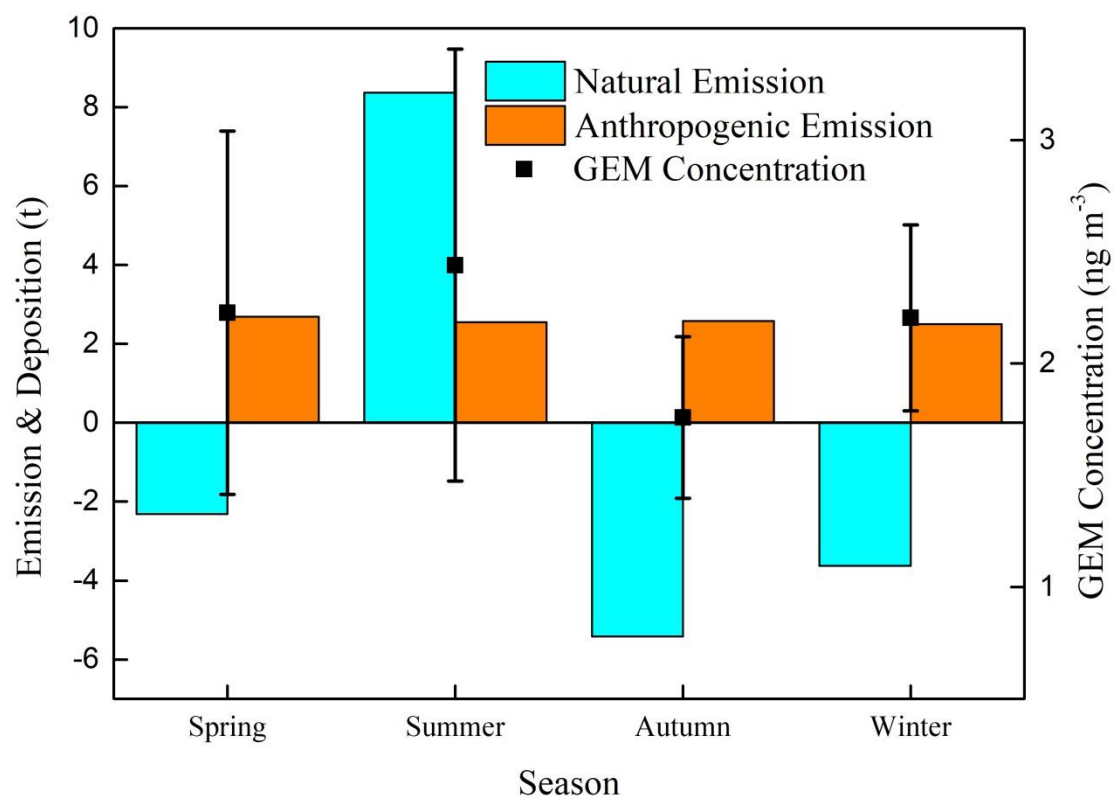


Figure 3. Monthly variations of GEM concentration at remote sites in China

607
608
609

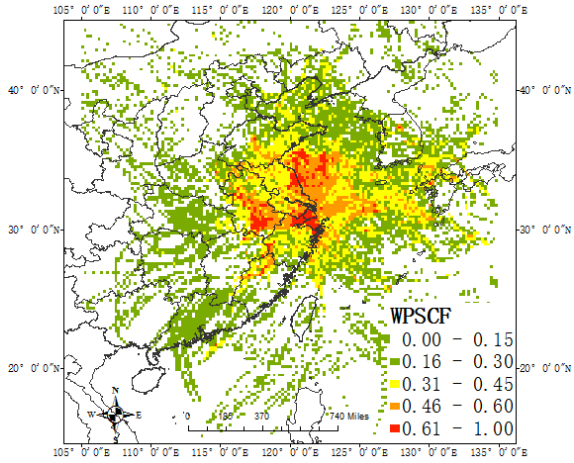
610



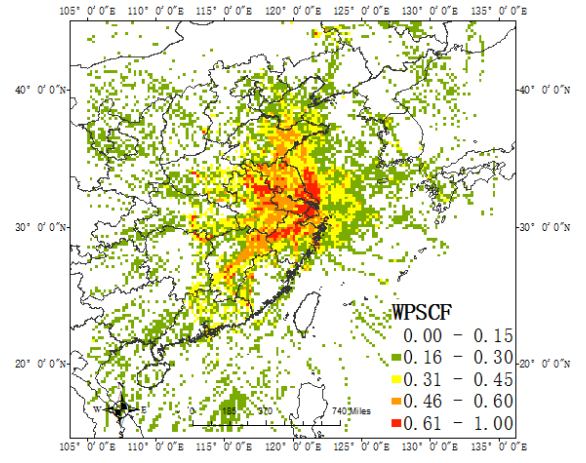
611

612 **Figure 4.** Seasonal cycle of GEM concentrations, anthropogenic and natural emissions during 2014-
613 2016. The error bars represent the standard deviation of seasonal average. Positive values of natural
614 emissions represent Hg emitted to air. Otherwise, negative values represent Hg deposition.

615



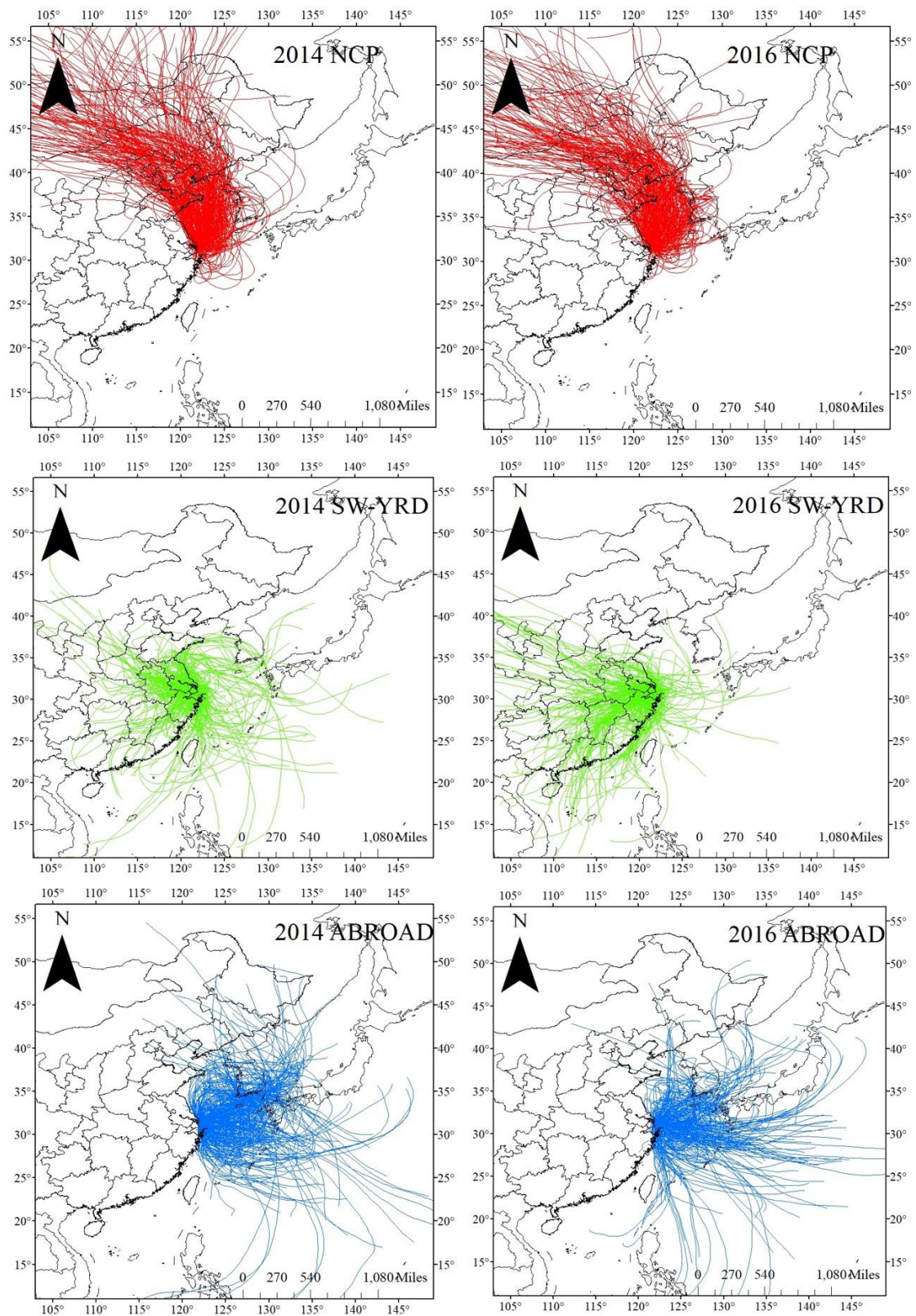
(a) 2014



(b) 2016

Figure 5. Source regions of GEM at monitoring site from PSCF model in 2014(a) and 2016(b)

616
 617
 618
 619



620

(a) 2014

(b) 2016

621

Figure 6. The back trajectories map for cluster NCP, SW-YRD and ABROAD in 2014(a) and

622

2016(b)

623

(NCP – North China Plain; SW-YRD – Southwest region and Yangtze River Delta; ABROAD –

624

Abroad)

Table 1. PCA component loading of GEM and other air pollutants

Air pollutants	2014		Air pollutants	2016	
	Factor 1	Factor 2		Factor 1	Factor 2
SO ₂	0.76	0.14	SO ₂	0.82	-0.09
NO _x	0.76	-0.20	NO _x	0.70	-0.52
O ₃	-0.11	0.98	O ₃	-0.41	0.97
PM _{2.5}	0.85	0.05	PM _{2.5}	0.88	0.05
GEM	0.66	0.02	GEM	0.78	-0.19
CO	0.79	0.12			
Component	Combustion	Transport of air mass from stratosphere	Component	Combustion	Transport of air mass from stratosphere
Variance explain (%)	49.36	17.53	Variance explain (%)	50.63	25.10

Note: Text in bold phase were regarded as high loading (factor loading > 0.40 or < -0.40)

628

Table 2. Emissions of the main air pollutants in YRD region in 2014

Emission sectors	Annual emissions			
	SO ₂ (kt)	NO _x (kt)	PM _{2.5} (kt)	GEM (t)
Coal-fired power plants	918.31	991.62	118.42	14.00
Coal-fired industrial boilers	311.03	271.94	79.91	9.80
Residential coal combustion	68.48	42.11	163.93	0.40
Cement clinker production	207.48	371.13	208.02	4.70
Iron and steel production	480.97	142.80	169.84	2.30
Mobile oil combustion	38.43	1786.74	98.00	1.90
Other sectors	348.83	316.28	382.48	2.50

629

630

631

632

Table 3. The statistics of cluster and estimated contribution of GEM reduction in 2014 and 2016

Time	Cluster	Trajectories			GEM concentration, C_j (ng m ⁻³)	Trajectory weighted concentration, TWC_j ,(ng m ⁻³)	Contribution to GEM reduction , CR_i
		Numbers	Ratio	Average Ratio (AR)			
2014	NCP	285	33%	32%	2.33	0.79	
	SW-YRD	304	35%	37%	3.19	1.18	
	ABROAD	275	32%	31%	2.58	0.77	
2016	NCP	237	31%	32%	1.48	0.50	26%
	SW-YRD	302	39%	37%	1.87	0.69	44%
	ABROAD	230	30%	31%	1.44	0.43	30%